Research Square

Preprints are preliminary reports that have not undergone peer review.
They should not be considered conclusive, used to inform clinical practice,
or referenced by the media as validated information.

Electrochemical Synthesis of Reduced Graphene Oxide Nanoparticles, Their MPS Functionalization and Their Effect on the Optical and Thermal Properties of a Non- Imprinted Methacrylic Polymer Nanocomposite

Mansour Bayati

mansourk.ali@uokufa.edu.iq

University of Kufa

Mustafa Abdulkadhim Hussien

University of Kufa

Research Article

Keywords: Reduced graphene oxide, electrochemical synthesis, polymer nanocomposite, thermal stability, optical properties

Posted Date: November 20th, 2026

DOI: https://doi.org/10.21203/rs.3.rs-11543162/v1

License: This work is licensed under a Creative Commons Attribution 4.0 International License.
Read Full License

Additional Declarations: No competing interests reported.

Electrochemical Synthesis of Reduced Graphene Oxide Nanoparticles, Their MPS Functionalization and Their Effect on the Optical and Thermal Properties of a Non-Imprinted Methacrylic Polymer Nanocomposite

Mansour Bayati[*1], Mustafa Abdulkadhim Hussien[2]
[1,2]Department of Chemistry, College of Science, University of Kufa, Najaf, Iraq

[1*]Corresponding author: mansourk.ali@uokufa.edu.iq

Abstract— A novel electrochemical method was used to synthesize reduced graphene oxide nanoparticles (rGO NPs) from graphite electrodes in a mixture of sulfuric acid and phosphoric acid. The rGO was functionalized with 3-(trimethoxysilyl)propyl methacrylate (MPS) and the functionalized rGO was embedded in a methacrylic acid (MAA)/ethylene glycol dimethacrylate (EGDMA) matrix to create an rGO@MPS/NIP nanocomposite polymer (NCP). The reduced graphene oxide was found to contain few layer nanosheets with a crystallite size between 18 and 53 nm by X-ray diffraction (XRD) analysis. The degree of purity (94.73% carbon, 4.94% oxygen and 0.32% sulfur) was confirmed by the energy-dispersive X-ray (EDX) analysis, and the zeta potential was measured as -1.13 mV. After the surface was functionalized by MPS the EDX analysis showed the presence of silicon (0.40 wt%), and the zeta potential was shifted towards more negative value (-1.37 mV) confirming successful modification of the surface. The nanocomposite polymer (NCP) showed peaks in its XRD pattern between 13.9° and 68.7° with crystallite sizes of 19 to 54 nm. Thermogravimetric analysis (TGA) showed that the onset of primary decomposition stage increased by 37.45 °C from 179.70 °C for the non-reinforced polymer (NIP) to 217.15 °C for the reinforced polymer (NCP) and the temperature of maximum decomposition was relatively close (408.94 °C versus 415.77 °C). The results presented herein show that the MPS functionalized reduced graphene oxide is a good nanofiller to improve the optical and thermal properties of methacrylate polymers.

Keywords: Reduced graphene oxide; electrochemical synthesis; polymer nanocomposite; thermal stability; optical properties.

1. Introduction

Polymers are macromolecules made up of repeating monomeric units (meres), which are connected to each other by covalent bonds. Due to their properties (including low density, ease of fabrication, chemical versatility, and low cost), they have been essential materials in various applications such as coatings, electronics, biomedicine, and analytical chemistry[1]. Of functional polymers, cross-linked methacrylic networks, prepared by the free-radical polymerization of a functional monomer (such as methacrylic acid, MAA) and a cross-linking agent (such as ethylene glycol dimethacrylate, EGDMA) are of special interest and are the base of molecularly imprinted polymers (MIPs) [2]. The functional monomer and cross-linking agent are polymerized around a template molecule during MIPs formation and the template is thereafter removed, creating cavities complementary to the target molecule in terms of size, shape and functionality [3]. The non-imprinted polymer (NIP) made without the template is used as the reference material for the intrinsic properties of the polymer matrix. These polymers have many applications as recognition elements of optical, electromagnetic, piezoelectric and thermal sensors, thanks to their low cost, ease of preparation and stability in extreme conditions [4]. But the organic polymer networks have very limited thermal stability, a poor light absorption, and low electrical conductivity, which limit their use in applications where high-performance properties are essential.

To overcome these limitations, nanomaterials, materials with at least one dimension below some 100 nanometers in size, provide a useful solution [1]. Depending on their size, they can be divided into zero-dimensional nanostructures (quantum dots, fullerenes, metal nanoparticles, etc.), one-dimensional nanostructures (nanotubes, nanowires, nanofibers, etc.), two-dimensional nanostructures (graphene, graphene oxide, reduced graphene oxide, layered double hydroxides, etc.), and three-dimensional nanostructures (graphene networks, and bundles of nanowires or nanotubes, etc.) [2]. Their characteristics, which include a high surface-area-to-volume ratio, surface charge, and size-dependent physical, chemical and optical properties, enable them to be modified and tailored for their specific application [3]. The polymer nanocomposites prepared by dispersing the nanofillers in a polymer matrix have enhanced properties even when the nanofiller concentration is very low due to the large surface area of the nanofiller in the polymer matrix, which limits the mobility of polymer chains and boosts the thermal and mechanical stability of the matrix[4]. Lamellar fillers act as barriers to slow the rate of heat transfer and release of volatile decomposition products from the matrix, where as conjugated or conductive fillers offer pathways for light absorption and electrical conduction that is not present in the neat polymer[5]. The amount of these enhancements is highly dependent on how well the nanofiller is dispersed and bonded to the matrix; in many cases, a coupling agent is used to modify the surface of the nanofiller. The methacrylate polymers are especially appropriate for silane coupling agents like 3-(trimethoxysilyl)propyl methacrylate (MPS), as the methoxysilyl group reacts with hydroxyl groups on the filler surface and the methacrylate group can copolymerize with the monomers, thus forming covalent bonds between filler and polymer network [6].

Reduced graphene oxide (rGO) is a typical two-dimensional nanomaterial which is employed for this purpose. It is based on an sp^2-hybridized basal plane that is like the basal plane of graphene but with defects and oxygen-containing groups. This structure gives the material a quasi-graphene like mechanical, optoelectronic and conductive properties [7] with surface functionalization sites from the remaining -OH and -COOH groups. These properties make rGO an interesting material for sensing applications among others, and biological, environmental, catalytic, optoelectronic and energy-storage applications. Its performance in the composite material is greatly influenced by the manufacturing, functionalization and processing techniques used [8]. Hence, it is predicted that rGO could be added to a polymer matrix and so increase the thermal stability and optical response of the polymer[9] .

In this study, rGO nanoparticles were prepared by a simple electrochemical route, functionalized with MPS (to form rGO@MPS) and then embedded in a non-imprinted polymer (NIP) that was made of MAA/EGDMA to create a rGO@MPS/NIP polymer nanocomposite (PNC). To analyse the effect of the incorporation of rGO on the structural, optical and thermal properties, the materials were characterised by X-ray diffraction (XRD), energy-dispersive X-ray spectroscopy (EDX), Fourier-transform infrared spectroscopy (FTIR), zeta potential measurements, UV-Vis-NIR spectroscopy and thermogravimetric analysis (TGA).

2. Methods

2.1. Electrochemical Preparation of Reduced Graphene Oxide Nanoparticles (rGO NPs)

The electrochemical cell presented in Figure 1 was used to prepare reduced graphene oxide (rGO) nanoparticles and consisted of a pure graphite plate as anode, another pure graphite plate as cathode, a maximum voltage of 30 V and maximum current of 5000 mA adjustable DC power supply and a magnetic stirrer[10]. The cathodes and anodes were first washed with acetone and ethanol, and the electrode surfaces were then washed with deionized water to remove any surface impurities formed. In the electrochemical system, the cell was filled with a mixture of 66 mL of sulfuric and phosphoric

acid.The anode used was a pure graphite plate of dimensions 2 cm × 5 cm × 1 cm and the cathode was an inert graphite electrode of dimensions 2 cm × 5 cm × 1 cm, both placed vertically opposite each other in the electrolyte solution with 2 cm gap between them. The electrolysis process was carried out in an undivided cell with a voltage of 9-15 volts and a time of 4 minutes. A black suspension of the rGO nanoparticles has appeared after four minutes, as indicated in the figure 2. After 6 hours, the temperature of the cell was lowered to 20°C by adding 70 mL of cold deionized water containing 2 mL of 30% hydrogen peroxide, to stop the electrochemical deposition process. The black precipitate obtained was centrifuged (Figure 3) and washed with deionized water and ethanol several times to form rGO nanoparticles. Finally, precipitate was collected and dried with diethyl ether according to the procedure shown in figure 1[11]

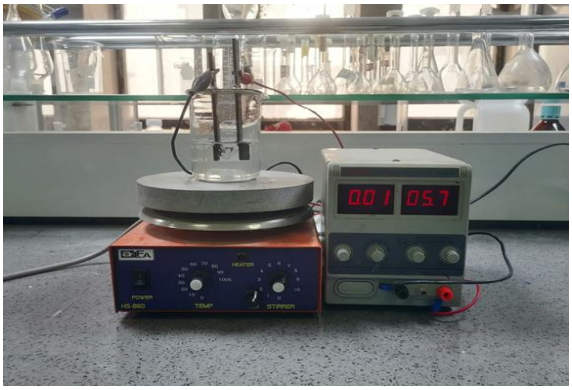


Figure 1. The electrochemical system for the preparation of rGO NPs.

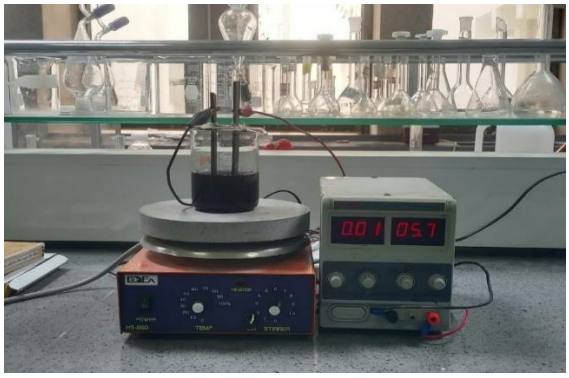


Figure 2**.** Suspension of rGO NPs formed during electrolysis.



Figure 3. Centrifugation process for separating rGO NPs.

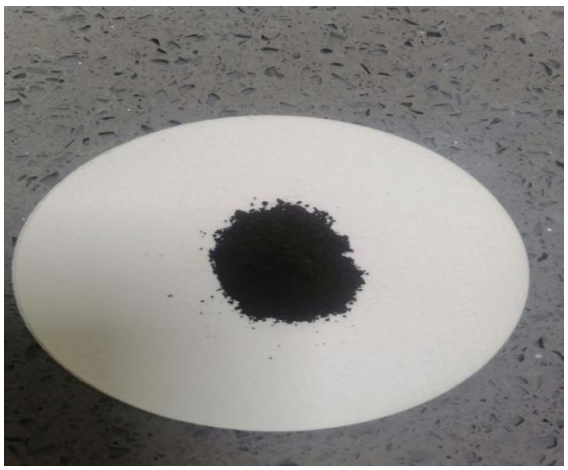


Figure 4. Precipitate of rGO NPs after drying.

2.2Activation of rGO NPs by 3-(Trimethoxysilyl)propyl Methacrylate (MPS)

To functionalize the reduced graphene oxide (rGO) nanoparticles, the first step was to dissolve 0.1 g of rGO in a solution of 90 mL of ethanol and 10 mL of deionized water, then sonicate for 30 minutes, as shown in Figure 5. Subsequently, 0.1 M hydrochloric acid was used to precisely adjust the pH to 5. After this, 1 mL of MPS was introduced per 0.1 g of rGO and the reaction was carried out at room temperature to stir for 24 hours. Finally, the precipitate was separated by centrifugation, washed three times with ethanol and dried at 60°C [12].



Figure 5. Sonication of rGO NPs.

2.3. Preparation of the Non-Imprinted Nanocomposite Polymer (rGO@MPS/NIP NCP)

MPS modified reduced graphene oxide (rGO–MPS) was dispersed in 3 mL of $CHCl_3$ with ultrasonication to obtain a uniform suspension. Then, 0.08 mL methacrylic acid (MAA) was added as a functional monomer, and stirred for 30 minutes. Then 0.15 mL of ethylene glycol dimethacrylate (EGDMA) was added as a cross-linking agent and 0.017 g of azobisisobutyronitrile (AIBN) was added, mixed at room temperature to remove the dissolved oxygen, and then polymerized in a water bath. The resulting polymer was collected and washed multiple times with ethanol and acetonitrile to remove unreacted monomers and impurities followed by drying at 60°C and storing in desiccator for further characterization. No template molecule was added during polymerization so the material obtained was named rGO–NIP[12] .

3. Results and Discussion

3.1. Characterization of rGO NPs

3.1.1. X-Ray Diffraction (XRD) Analysis of rGO NPs

A diffraction system with Cu-Kα1 radiation (wavelength, λ = 1.54060 Å) was used to analyze rGO NPs at 40 kV and 30 mA over the diffraction angle (2θ) range of 10° to 80°. The X-ray diffraction (XRD) pattern of the nanoparticles (Figure 6) revealed several diffraction peaks at 2θ values of 12.6°, 13.8°, 20.0°, 23.3°, 26.6°, 31.8°, 34.9°, 40.2°, 42.5°, 45.3°, 50.1°, 59.7°, 67.5°, 73.0°, 76.2°, and 78.2°; the broad peaks (at 26.6° and 42.5°) indicate the presence of a few layers of reduced graphene oxide (rGO) sheets within the particles[13] .

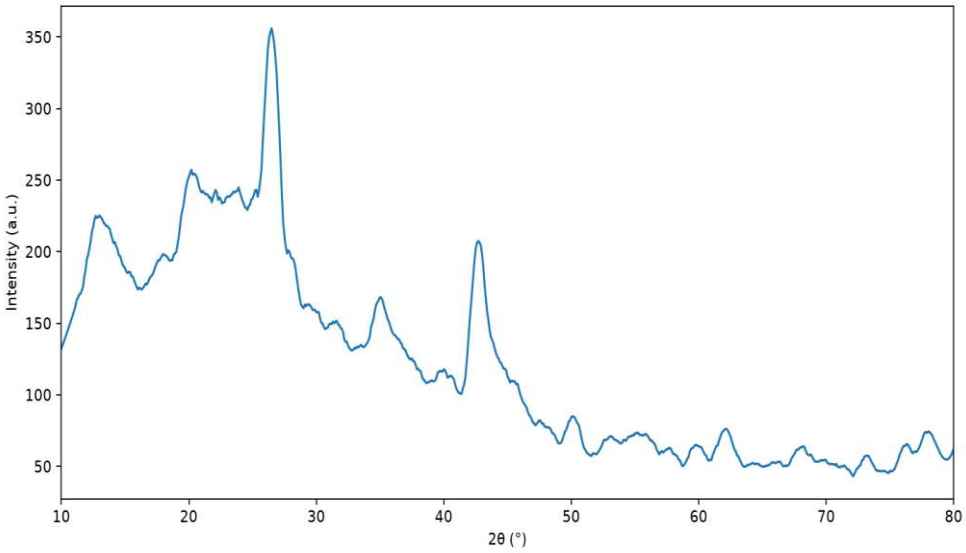


Figure 6. XRD pattern of rGO NPs.

3.1.2. Energy-Dispersive X-Ray Spectroscopy (EDX) of rGO NPs

The measurements of energy-dispersive X-ray (EDX) spectroscopy are carried out to check the purity and elemental composition (stoichiometry) of the electrochemically produced reduced graphene oxide (rGO) nanoparticles, confirming the high purity of the sample with only carbon, sulfur and oxygen signals. As shown in Figure 7, the weight percentages for the rGO sample were: Carbon (C) = 94.73%, Oxygen (O) = 4.94%, and Sulfur (S) = 0.32%. The extremely high carbon content itself corroborates the successful electrochemical reduction of graphene oxide, which can be explained by the restoration of the sp^2 carbon conjugation network. In the electrochemical reduction - cooling with hydrogen peroxide (H_2O_2) process, most of the oxygen containing compounds are eliminated. The GO basal plane was successfully removed of both functional groups (–OH, C=O) and also the –COOH and epoxide C–O–C bridges. During this deoxygenation process, the aromatic π–π conjugated carbon lattice, typical of rGO[14] is recovered.

Spectrum: Acquisition

Element	Series	unn. C [wt.%]	norm. C [wt.%]	Atom. C [at.%]	Error (1 Sigma) [wt.%]
Carbon	K-series	94.73	94.73	96.11	13.04
Oxygen	K-series	4.94	4.94	3.77	1.26
Sulfur	K-series	0.32	0.32	0.12	0.04
Total:		100.00	100.00	100.00	

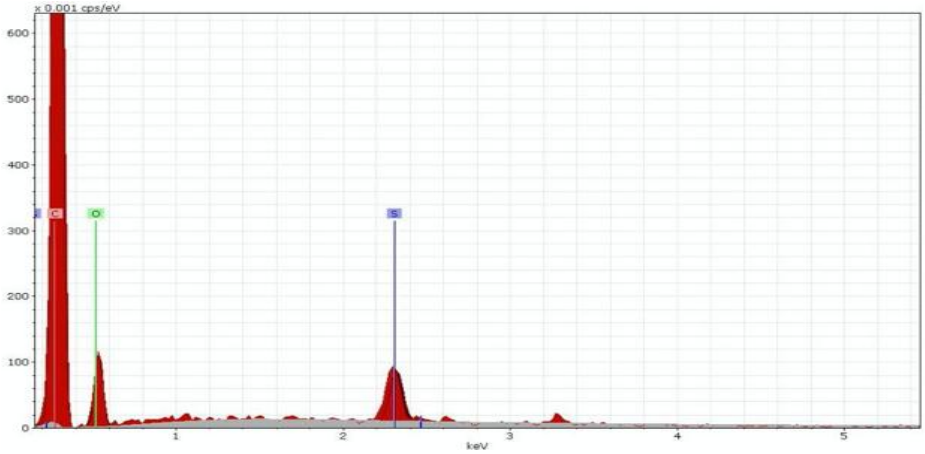


Figure 7. EDX spectrum and elemental composition of rGO NPs.

3.1.3. Fourier-Transform Infrared (FTIR) Spectroscopy of rGO NPs

To identify the surface chemical groups present on the electrochemically prepared reduced graphene oxide (rGO) nanoparticles, Fourier-transform infrared (FTIR) spectroscopy was used. The FTIR spectrum of the synthesized rGO was recorded in the range of 4000–400 cm^{-1} using a Bruker FT–IR spectrometer (Figure 8) and the assignments of the peaks in the spectrum are summarized in Table 2[15].

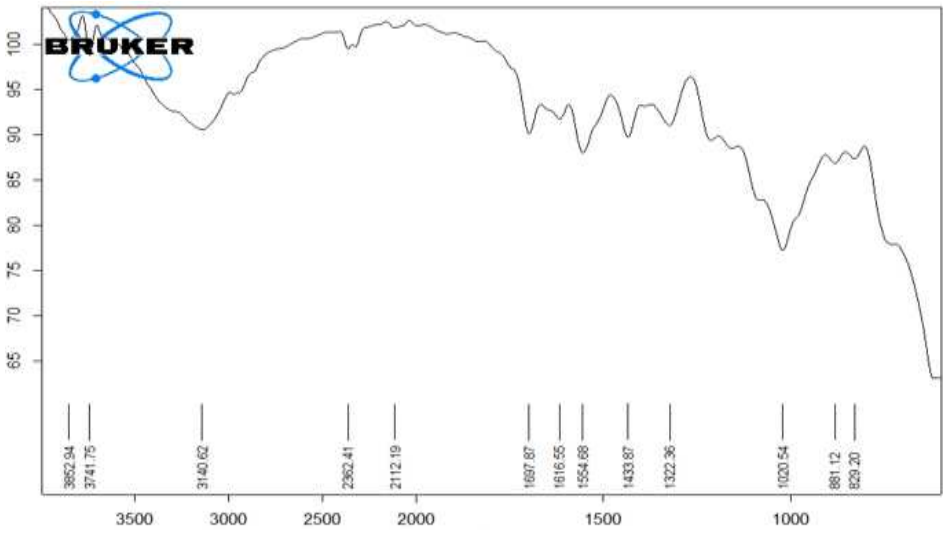


Figure 8. FTIR spectrum of rGO NPs.

3.1.4. Zeta Potential of rGO NPs

The Z-average potential of rGO sample was measured with HORIBA SZ-100 analyzer. Since the measurement was performed three times to ensure statistical stability, values of -1.0, -1.2 and -1.1 mV with an average value of -1.13 mV were obtained, which corresponds to functional groups of -OH and -COOH groups on the surface of rGO. The distribution curve (shown in Figure 9) shows that the

distribution is uniform with a single sharp, symmetrical peak in the vicinity of zero, consistent with the average value recorded.

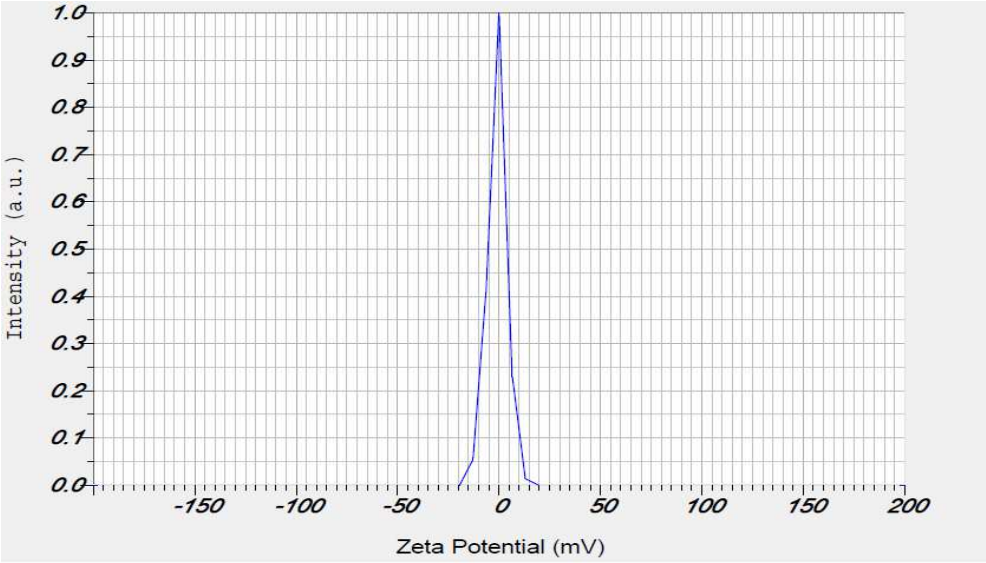


Figure 9. Zeta potential distribution of rGO NPs.

3.2. Characterization of MPS-Activated rGO (rGO@MPS NPs)

3.2.1. XRD Analysis of rGO@MPS NPs

The X-ray diffraction (XRD) pattern of rGO@MPS nanoparticles was captured using Cu-Kα_1 radiation (wavelength λ = 1.540598 Å) at a voltage of 50 kV and current of 40 mA for an angle range of (2θ) 10–80°. Sharp diffraction peaks for the synthesized rGO@MPS nanoparticles were observed at the following 2θ values: 17.123°, 21.409°, 26.695°, 29.564°, 32.437°, 34.21°, 39.105°, 49.837°, 62.055°, and 79.21° (as shown in Figure 10 and Table 3); these values are characteristic of these nanoparticles. The variation of XRD pattern of rGO@MPS nanoparticles from the pristine rGO nanoparticles can be explained by the difference in the chemical composition and structural properties of the material which was caused by the functionalization process with the compound of MPS.

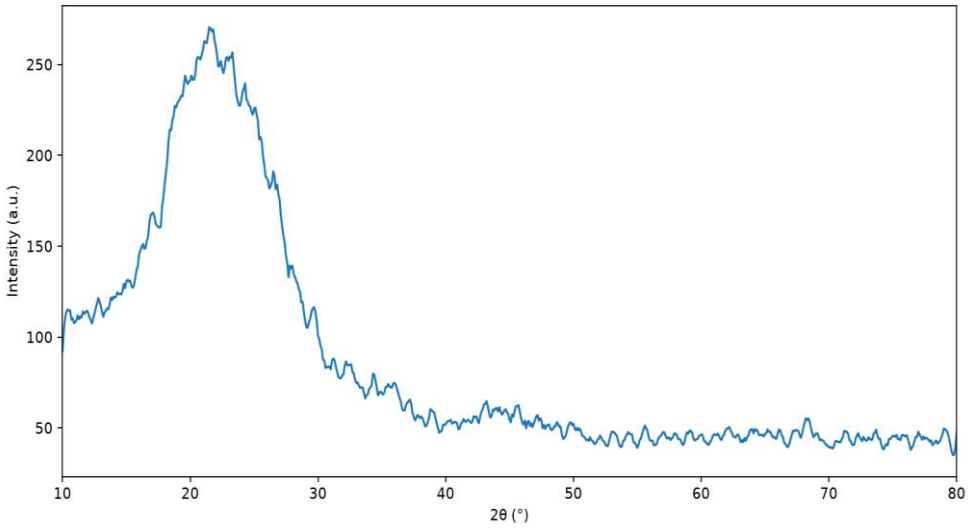


Figure 10. XRD pattern of rGO@MPS NPs.

3.2.2. EDX Analysis of rGO@MPS NPs

The purity of the rGO@MPS nanoparticles was determined with the aid of a rGO. The results shown in figure 11 demonstrate that the samples are very pure because only signals from oxygen, sulfur, silicon and carbon are present. The total weight percentages were as follows: carbon (91.96%), oxygen

(6.80%), silicon (0.40%), and sulfur (0.84%). The unique silicon signal is especially important because silicon is one of the building blocks of MPS' silane compound—proof of the successful surface functionalization of the rGO nanoparticle with MPS. Moreover, the presence of the characteristic elements of the prepared rGO@MPS material, without the presence of any additional elements, signifies the material's high purity.

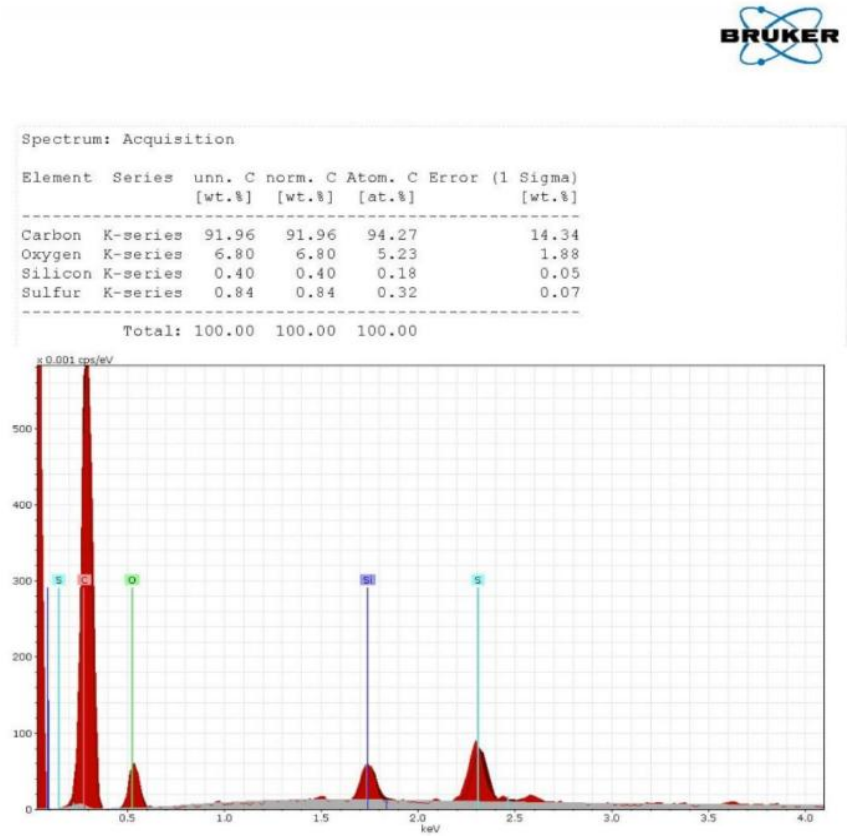


Figure 11. EDX spectrum and elemental composition of rGO@MPS NPs.

3.2.3. FTIR Analysis of rGO@MPS NPs

FT-IR spectroscopy can be used to detect the functional group of material. The interaction of electromagnetic radiation with the functional groups of the material means that, if the material does have more than one functional group, then a number of different signals can be obtained in the spectrum [16]. The FTIR spectrum of prepared rGO@MPS nanoparticles revealed certain absorption bands corresponding to the functionalizing agent of MPS (1146.62, 977.39, 874.42 and 810.09) [17] as shown in Figure 12.

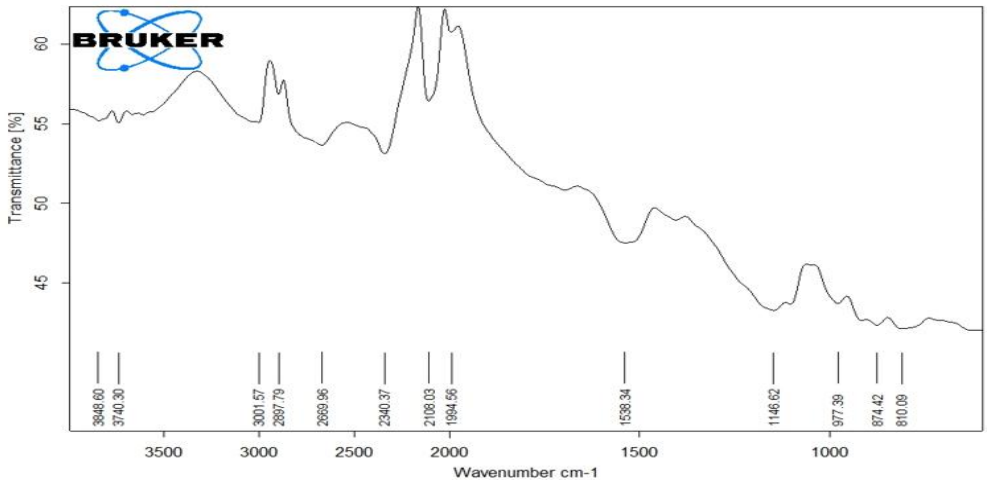


Figure 12. FTIR spectrum of rGO@MPS NPs.

3.2.4. Zeta Potential of rGO@MPS NPs

The Zeta potential of the rGO@MPS sample was measured using the HORIBA SZ-100 analyzer. The measurements were carried out in triplicate to obtain statistical reliability, and the obtained results were -1.3, -1.4 and -1.4 mV with an average zeta potential of -1.37 mV. The distribution curve (Figure 13) shows a single, sharp, and symmetrical peak centred around a charge value near zero which is consistent with the average value and uniformity of charge distribution across the particle population as noted previously.The zeta potential of rGO@MPS was found to be more negative compared to that of the un-modified rGO sample (-1.37 mV vs -1.13 mV). The successful surface modification of rGO using MPS was believed to be responsible for this increase in the negative surface charge, as it added extra polar/ionizable groups, including silanol (Si-OH) group, and thiol (-SH) group. The gradual increase of the negative charge during the three measurements is a proof of the successful immobilization of MPS on the surface of reduced graphene oxide (rGO) [18].

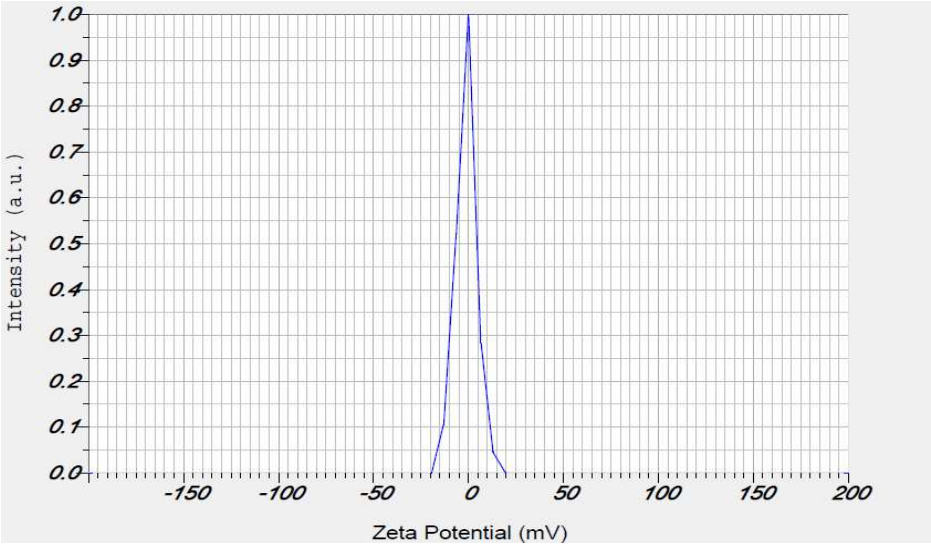


Figure 13. Zeta potential distribution of rGO@MPS NPs.

3.3. Characterization of the Non-Imprinted Nanocomposite Polymer (rGO@MPS/NIP NCP)

3.3.1. XRD Analysis of rGO@MPS/NIP NCP

The X-ray diffraction (XRD) pattern of the rGO@MPS/NIP nanocomposite was obtained, using Cu-$K\alpha_1$ radiation at 50 kV and 40 mA with a diffraction angle (2θ) range from 10° to 80°. The pattern exhibits peaks at 2θ values of 13.9°, 15.7°, 18.9°, 30.7°, 34.3°, 39.5°, 48.0°, 56.7°, and 68.7° as shown in Figure 14 , with crystallite sizes ranging from 19 to 54 nm, calculated using the Scherrer equation. The difference in the XRD pattern between rGO@MPS/NIP nanoparticles and rGO@MPS/MIP composite can be explained by the difference in the structure of the composite; in the absence of the methamphetamine (MAA) molecule in the polymerization process the methacrylic acid (MAA) monomers and cross linking agent (EGDMA) form a completely random network around the surface of the rGO@MPS. This leads to a more amorphous and homogeneous polymer matrix, devoid of the order in which the template has built. The distribution of local organization in the crosslinked network varies in the MIP case, in contrast to the latter, as is evident from the shapes and intensities of the peaks in the diffraction pattern.

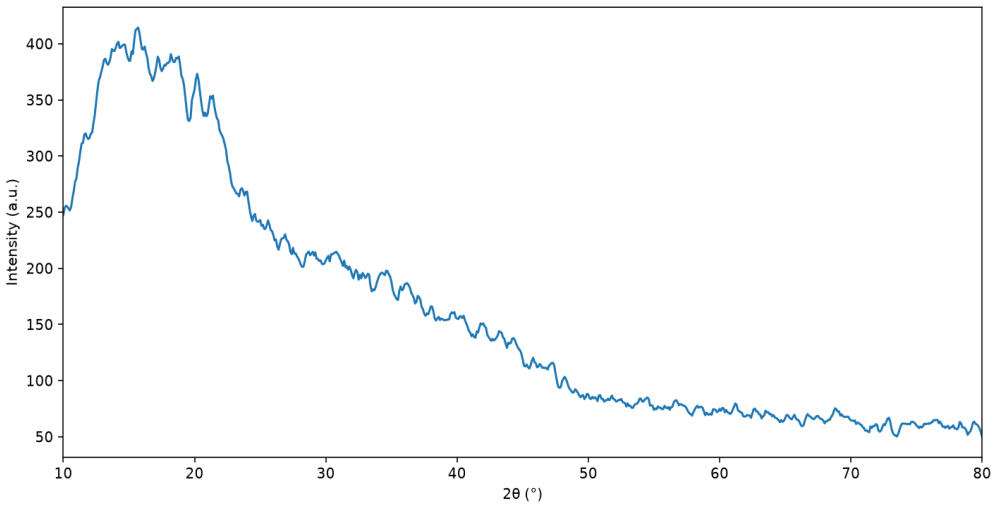


Figure 14. XRD pattern of rGO@MPS/NIP NCP.

3.3.2. FTIR Analysis of rGO@MPS/NIP NCP

The Fourier-transform infrared (FTIR) spectrum of the rGO@MPS/NIP nanocomposite (NCP) was recorded using a Bruker spectrometer in the range of 4000 to 400 cm^{-1}. The spectrum exhibits characteristic absorption bands confirming the successful incorporation of all components into the nanocomposite structure, as shown in Figure 15 .

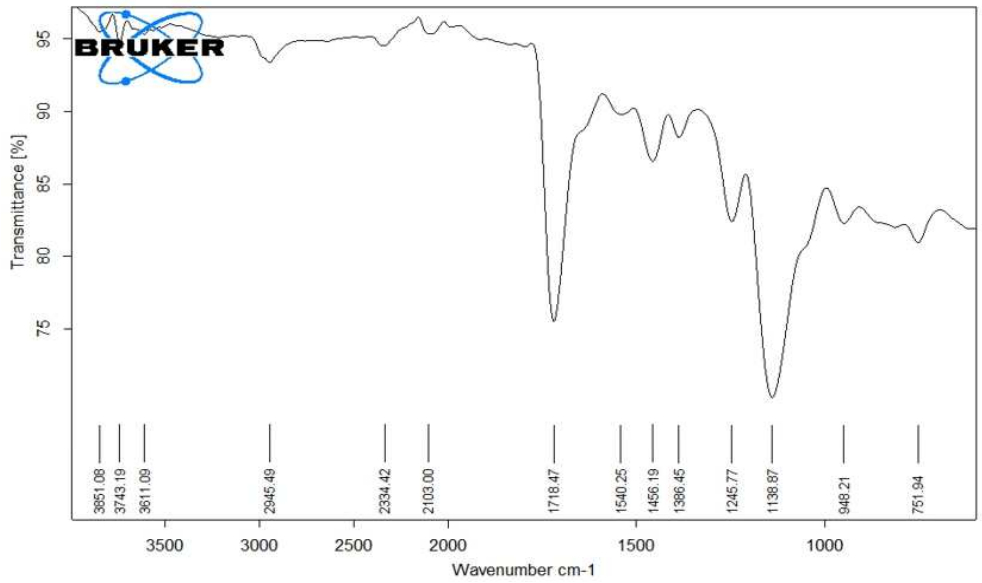


Figure 15. FTIR spectrum of rGO@MPS/NIP NCP.

3.3.3. UV–Vis–NIR Spectroscopy of rGO@MPS/NIP NCP and NIP

Thin films of NCP rGO@MPS/NIP were prepared on glass slides at temperatures below 300°C and analyzed using solid-state UV-Vis spectroscopy. The resulting spectra (shown in Figure 16) exhibit a characteristic peak wavelength. The most substantial increase was observed in the visible light range, indicating that the incorporation of rGO significantly modified and broadened the polymer's optical response. This enhanced response extended across the ultraviolet, visible, and near-infrared regions, consistent with the broad optical contribution of the rGO-containing polymer.

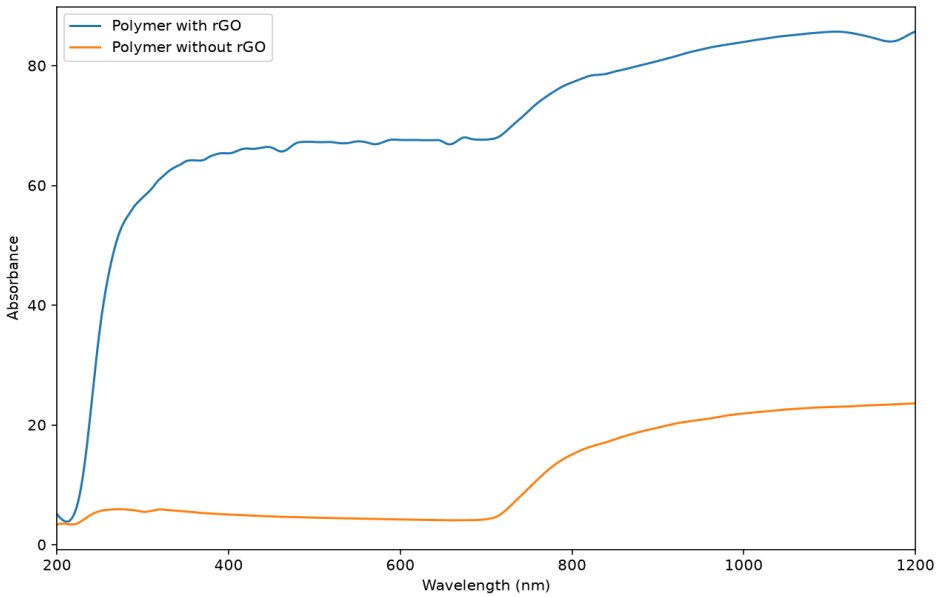


Figure 16. UV–Vis–NIR absorption spectra of the non-imprinted polymers with rGO (rGO@MPS/NIP NCP) and without rGO (NIP).

As shown in Figure 16, the rGO@MPS/NIP composite nanoparticles exhibited a significantly more intense and broader spectral response compared to the NIPs across most of the studied wavelength range. While the NIP nanoparticles displayed a characteristic absorption feature at a wavelength of approximately 272 nm, the incorporation of rGO resulted in a marked enhancement extending from the ultraviolet (UV) region into the visible and near-infrared (NIR) ranges. This broadening and enhancement of the optical response indicate that the incorporation of rGO has a significant impact on the optical properties of the polymer matrix.

3.3.4. Thermogravimetric Analysis (TGA) of rGO@MPS/NIP NCP and NIP

Thermogravimetric analysis (TGA) showed a significant enhancement in the thermal stability of the polymer after rGO nanomaterial was added to it. The start temperature of the main decomposition process was increased by about 37.45 °C from approximately 179.70 °C (polymer without rGO) to 217.15 °C (polymer with rGO) (Figure 17 and 18). This increase in the decomposition onset temperature suggests that the introduction of the rGO nanomaterial affected the onset of the main thermal decomposition process. This improvement in thermal stability can be explained by the barrier effect that is created by the rGO nanosheets, which block the mobility of polymer chains and the diffusion of volatile decomposition products and heat in the polymer matrix. In addition, the surface of rGO could interact with the polymer network, which could be a potential mechanism for improving thermal durability. The decomposition temperature peak for both samples were quite similar, with approximately 415.77°C and 408.94°C for rGO-free and rGO-containing polymers, respectively. The big effect of rGO on the investigated system is, therefore, in the delay of the main thermal degradation temperature and not in a significant shift in the peak of the temperature of degradation.

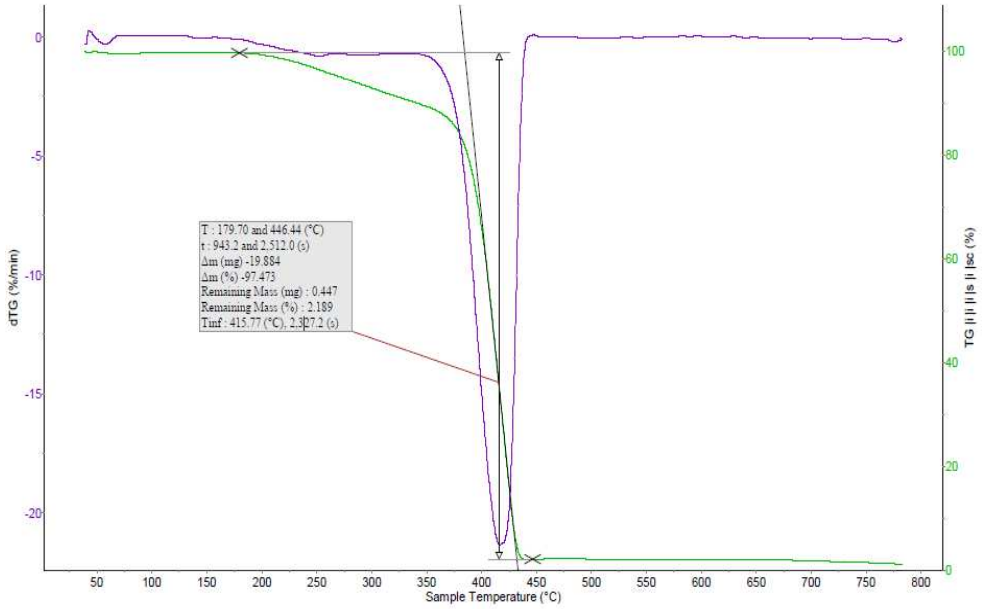


Figure 17. TGA/DTG curves of the non-imprinted polymer without rGO (NIP).

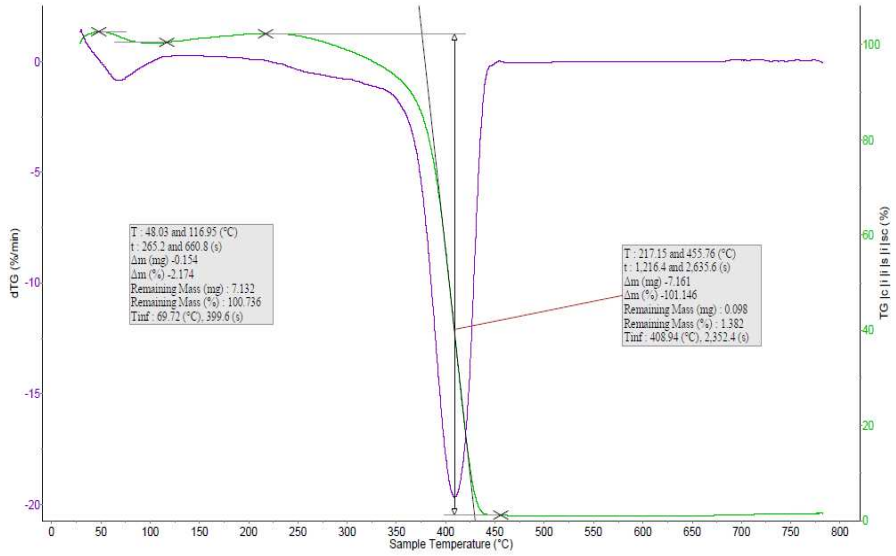


Figure 18. TGA/DTG curves of the non-imprinted polymer with rGO (rGO@MPS/NIP NCP).

4. Conclusions

The simple and rapid electrochemical method was used to successfully prepare reduced graphene oxide (rGO) nanoparticles (with 4 minutes of electrolysis). The product was found to be high purity (94.73 wt% carbon), was few-layered with the crystallite size in the range of 18–53 nm, showed restored sp^2 carbon network (C=C band at 1616 cm^{-1}) and a slightly negative surface charge (-1.13 mV). MPS was also successfully grafted onto the rGO surface by detecting Si atom (0.40 wt%) using EDX analysis, FTIR bands for Si–O–C, Si–O–Si and Si–OH, changes in X-ray diffraction (XRD) pattern and also in the negative zeta potential (-1.37 mV). The rGO@MPS nanoparticles were embedded into the polymer network of MAA/EGDMA; the FTIR analysis showed characteristic peaks for rGO, MPS, MAA, and EGDMA indicating that the polymer nanocomposite of rGO/MPS/MAA/EGDMA has been formed. The enhanced and extended optical response of the polymer was achieved by the addition of rGO. Moreover, the thermal stability of the polymer increased, as the onset temperature of the main degradation step increased by 37.45°C (from 179.70°C to 217.15°C), and the temperature of maximum decomposition did not change significantly. The barrier effect that the rGO nanosheets exert and their interaction with the polymer network, which

hampers the mobility of polymer chains and postpones the onset of decomposition, are the main reasons for this phenomenon. Therefore, the rGO@MPS/NIP nanocomposite can be used as a promising platform and suitable reference material for the molecularly imprinted polymer (MIP) development with improved optical and thermal properties for sensing applications.

-Declarations

-Author Contributions

Mansour Bayati: conceptualization, methodology, investigation, formal analysis, data curation, visualization, writing – original draft. Mustafa Abdulkadhim Hussien: conceptualization, supervision, validation, resources, project administration, writing – review and editing. All authors have read and agreed to the published version of the manuscript.

-Funding

This research received no external funding.

-Conflicts of Interest

The authors declare no conflict of interest.

-Data Availability Statement

The data supporting the findings of this study are available from the corresponding author upon reasonable request.

-Ethical Approval

Not applicable. This study did not involve human participants or animals.

-Acknowledgments

The authors gratefully acknowledge the Department of Chemistry, College of Science, University of Kufa, Najaf, Iraq, for providing the laboratory facilities and support that made this work possible.

Declaration of Generative AI Use

During the preparation of this manuscript, the authors used an AI tool to reorganize the manuscript and improve its language.

5.References

1. Khizar, S., et al., Electrochemical Sensors for Enhanced and Rapid Detection of Illicit Drugs. Electroanalysis, 2025. 37(3): p. e12034. doi.org/10.1002/elan.12034
2. Tse Sum Bui, B., A. Mier, and K. Haupt, Molecularly imprinted polymers as synthetic antibodies for protein recognition: the next generation. Small, 2023. 19(13): p. 2206453. doi.org/10.1002/smll.202206453
3. Haupt, K., P.X. Medina Rangel, and B.T.S. Bui, Molecularly imprinted polymers: antibody mimics for bioimaging and therapy. Chemical reviews, 2020. 120(17): p. 9554-9582. doi/10.1021/acs.chemrev.0c00428.
4. Hashim, P. and S.S.M.A. Abdrabou, Sub-100 nm carriers by template polymerization for drug delivery applications. Nanoscale Horizons, 2024. 9(5): p. 693-707. doi.org/10.1039/d3nh00491k
5. Selvolini, G. and G. Marrazza, Sensor principles and basic designs, in Fundamentals of Sensor Technology. 2023, Elsevier. p. 17-43. doi/10.1016/B978-0-323-88431-0.00018-1
6. Lee, B., Duong, C.N., Cho, J., Lee, J., Kim, K., Seo, Y., Kim, P., Choi, K., and Yoon, J., Toxicity of citrate-capped silver nanoparticles in common carp (Cyprinus carpio). Journal of Biomedicine and Biotechnology, 2012. 2012: p. 262670. doi.org/10.1155/2012/262670
7. Al-Byati, M.K.A.A. and A.M.J. Al-Duhaidahawi, Synthesis and characterization of zinc oxide nanoparticles by electrochemical method for environmentally friendly dye-sensitized solar cell applications (DSSCs). Biomedicine and Chemical Sciences, 2023. 2(1): p. 53-57. doi.org/10.48112/bcs.v2i1.348

8. Kam, O., et al., Low-Cost Synthesis of Alumina Nanoparticles and Their Usage for Bisphenol-A Removal from Aqueous Solutions. Processes 2021, 9, 1709. 2021, s Note: MDPI stays neutral with regard to jurisdictional claims in published. doi.org/10.3390/pr9101709
9. Chee, P., et al., Introduction of nanotechnology and sustainability. 2022.
10. Vinukonda, A., et al., Synthesis of nanoparticles using advanced techniques. Next Nanotechnology, 2025. 8: p. 100169. doi.org/10.1016/j.nxnano.2025.100169
11. Zahoor, M., et al., Electrochemical synthesis of nanoparticles; an appropriate contrivance of synthesizing nanoparticles with low dimensional structures. Inorganic Chemistry Communications, 2025: p. 113890. doi.org/10.2147/IJN.S562203
12. Masteri-Farahani, M., S. Mashhadi-Ramezani, and N. Mosleh, Molecularly imprinted polymer containing fluorescent graphene quantum dots as a new fluorescent nanosensor for detection of methamphetamine. Spectrochimica Acta Part A: Molecular and Biomolecular Spectroscopy, 2020. 229: p. 118021. doi /10.1016/j.saa.2019.118021
13. Gupta, B., et al., Role of oxygen functional groups in reduced graphene oxide for lubrication. Scientific reports, 2017. 7(1): p. 45030. doi.org/10.1038/srep45030
14. Narayan, P.S., et al., Eco-friendly reduced graphene oxide for the determination of mycophenolate mofetil in pharmaceutical formulations. Journal of Pharmaceutical Analysis, 2018. 8(2): p. 131-137. doi.org/10.1016/j.jpha.2017.12.001
15. Kamau, M., S. Al-Najm, and M. Nandeshwar, Recent advances in carbon-based nanocomposites for environmental remediation of industrial dyes. Composite Interfaces, 2026. 33(3): p. 567-600.doi.org/10.1080/09276440.2025.2534741
16. Koczoń, P., et al., The analytical possibilities of FT-IR spectroscopy powered by vibrating molecules. International Journal of Molecular Sciences, 2023. 24(2): p. 1013. doi.org/10.3390/ijms24021013
17. Masmoudi, M., Electrochemical Study of Silanes Grafted into Surface of Copper. Thin Films, 2021: p. 29.
18. Chowdury, M.S.K., et al., Nanohybrid graphene oxide membranes functionalized using 3-mercaptopropyl trimethoxysilane for proton exchange membrane fuel cells. Journal of Membrane Science, 2022. 663: p. 121035. DOI 10.1149/1945-7111/acc35e
19. Kakakhel, M.A., Wu, F., Sajjad, W., et al., Long-term exposure to high-concentration silver nanoparticles induced toxicity, fatality, bioaccumulation, and histological alteration in fish (Cyprinus carpio). Environmental Sciences Europe, 2021. 33: p. 14. doi.org/10.1186/s12302-021-00453-7